c-axis resistivity of $SbCl_5$ graphite intercalation compounds

1997 J. Phys.: Condens. Matter 9 10399

(http://iopscience.iop.org/0953-8984/9/47/009)

J. Phys.: Condens. Matter **9** (1997) 10399–10420. Printed in the UK PII: S0953-8984(97)80087-2

c-axis resistivity of $SbCl_5$ graphite intercalation compounds

Masatsugu Suzuki†, Itsuko S Suzuki†, Chaoli Lee†, Ross Niver†, Keiko Matsubara‡ and Ko Sugihara§

† Department of Physics, State University of New York at Binghamton, Binghamton, NY 13902-6016, USA

‡ Department of Electrical Engineering, College of Science and Technology, Nihon University, Chiyoda-ku, Tokyo 101, Japan

§ College of Pharmacy, Nihon University, Funabashi, Chiba 274, Japan

Received 4 December 1996, in final form 27 May 1997

Abstract. The *c*-axis resistivity ρ_c of stage-2, 3, 4, 5, 6, 7, and 9 $SbCl_5$ graphite intercalation compounds (GICs) has been measured in the temperature range between 4.2 and 300 K with and without an external magnetic field along the *c*-axis. In these compounds the *c*-axis conduction is dominated by the in-plane conduction because of the highly anisotropic resistivity. The temperature dependence of ρ_c strongly depends on the stage number. The stage-2 and 3 $SbCl_5$ GICs show a metallic behaviour: ρ_c increasing with increasing temperature. The logarithmic behaviour in ρ_c is observed in a limited temperature range for stages 5 and 6, and negative longitudinal magnetoresistance is observed for stages 3 to 7, indicating that the two-dimensional weak localization effect may occur mainly in the interior graphite layers with a small charge transfer. The *c*-axis resistivity of stage-3 to 9 $SbCl_5$ GICs shows a unusual thermal hysteresis in the temperature range between 180 and 240 K. It has two local minima at critical temperatures T_{cl} (=196–210 K) and T_{cu} (=223–231 K) depending on the stage number. The carriers in the bounding graphite layers with a large charge transfer are scattered by enhanced fluctuations due to electric dipole moments of $SbCl_3$ molecules. There may occur a two-dimensional- (2D-) like dipole ordered phase below T_{cu} and a 3D-like dipole ordered phase below T_{cl}.

1. Introduction

The *c*-axis transport properties of acceptor-type graphite intercalation compounds (GICs) has recently stimulated extensive experimental [1–9] and theoretical studies [10–13]. In these compounds the *c*-axis resistivity ρ_c is much larger than the in-plane resistivity ρ_a:$\rho_c/\rho_a \approx 10^4$–$10^6$. Because of this high anisotropy in resistivity, the *c*-axis conduction is strongly influenced by the in-plane conduction. In a previous paper [14] we reported the experimental results on the *c*-axis resistivity ρ_c and longitudinal magnetoresistance (MR) for stage-2–6 $MoCl_5$ GICs. We observed (i) a logarithmic behaviour of ρ_c at low temperatures for stage-3, 4, and 5 $MoCl_5$ GICs and (ii) a negative longitudinal MR for stage-4 and 5 $MoCl_5$ GICs. These phenomena have been explained in association with two possibilities: a two-dimensional (2D) weak localization effect and a Kondo effect related to the exchange interaction between Mo^{5+} ions with spin $S = 1/2$ and spins of π electrons.

In this paper we report the experimental results on the *c*-axis resistivity ρ_c of stage-2–9 $SbCl_5$ GICs without and with an external magnetic field along the *c*-axis. We will show that ρ_c of $SbCl_5$ GICs has a variety of temperature and field-dependence varying with stage number: (i) a metallic behaviour of stage-2, 3, and 4 $SbCl_5$ GICs at low temperatures, (ii) a logarithmic behaviour of ρ_c in a limited temperature range for stage-5 and 6 $SbCl_5$ GICs,

0953-8984/97/4710399+22$19.50

(iii) a negative longitudinal MR at low magnetic fields for stage-3 to 7 $SbCl_5$ GICs, (iv) a semiconductor-like behaviour for stages 7 and 9 in the intermediate temperatures. Unlike Mo^{5+} in $MoCl_5$ GICs, the Sb ion has no spin. This implies that both logarithmic behaviour and negative MR are due to the 2D weak localization effect, but not due to the Kondo effect. We will also show a pronounced thermal hysteresis of ρ_c for $SbCl_5$ GICs with $3 \leqslant n \leqslant 9$ in the temperature range between 180 and 240 K. This strong hysteresis character in ρ_c against T is discussed in association with enhanced fluctuation due to electric dipole moments of $SbCl_3$ occurring in the intercalate layers of $SbCl_5$ GICs. The in-plane structure of $SbCl_5$ GICs is complicated by the incomplete disproportionation during the intercalation process [15–20]. Mössbauer studies [19, 20] and scanning transmission electron microprobe (STEM) [16] have clearly shown that there are $SbCl_3$, $SbCl_4^-$, $SbCl_5$, and $SbCl_6^-$ molecular species in $SbCl_5$ GICs. The $SbCl_6^-$ molecule is formed of a $(\sqrt{7} \times \sqrt{7})R \pm 19.1^\circ$ commensurate structure, while the $SbCl_3$ molecule is formed of the in-plane structure with a lattice constant approximately 2% compressed relative to that of the $(\sqrt{39} \times \sqrt{39})R \pm 16.1^\circ$ commensurate structure [17]. For $SbCl_5$ GICs with $n \geqslant 3$ the latter phase undergoes a first-order phase transition near 210–230 K, while the former phase remains unchanged.

There have been several works concerning the temperature (T-) dependence of ρ_c for $SbCl_5$ GICs [1, 2, 8, 9]. As far as we know there has been no report on the logarithmic behaviour of resistivity in these compounds. Morelli and Uher [1] have reported the results of ρ_c against T for stage-1–6 and 10 $SbCl_5$ GICs. (i) A metallic behaviour is observed for stage-1 to 3 $SbCl_5$ GICs over the entire temperature range. (ii) The higher-stage compounds ($n \geqslant 4$) show metallic character only at high temperatures: there occurs a crossover to a semiconductor-like behaviour with decreasing temperature. (iii) For $n \geqslant 2$ the resistivity shows an anomaly at 210 K. Andersson *et al* [8] have reported the results of ρ_c against T for stage-2–8 $SbCl_5$ GICs: an anomaly in ρ_c against T around 230 K for stage-3–8 $SbCl_5$ GICs accompanying a pronounced thermal hysteresis. This anomaly is interpreted in terms of structural change from a high-temperature phase with disordered or partly ordered in-plane structure to a low-temperature ordered phase with ordered in-plane structure.

The outline of this paper is as follows. In section 2 we will describe the experimental procedure. In section 3 we will show experimental results on the $(00L)$ x-ray diffraction, the c-axis resistivity, and the longitudinal MR for $SbCl_5$ GICs. In section 4 we will discuss the results of negative longitudinal MR, logarithmic behaviour, and first-order phase transition observed in the c-axis resistivity in the light of models proposed here.

2. Experimental procedure

$SbCl_5$ GIC samples were synthesized using a two-zone furnace, where the temperature of graphite (T_G) was kept constant at 225 °C and the temperature of $SbCl_5$ (T_I) was changed depending on the stage number. Highly oriented pyrolytic graphite (HOPG) and $SbCl_5$ are vacuum sealed in the Pyrex glass tubing. The values of T_G and T_I for each stage number were almost the same as those reported by Yosida *et al* [21]. We used the isotherm diagram of stage number in $SbCl_5$ GICs obtained when T_I is increased. The staging structure of $SbCl_5$ GIC samples was determined from $(00L)$ x-ray scattering measurements made at 295 K using a Huber double-circle diffractometer with an Mo Kα x-ray radiation source (1.5 kW) and HOPG monochromator.

The c-axis electrical resistivity of $SbCl_5$ GIC samples in the absence and the presence of an external magnetic field applied along the c-axis were measured in the temperature range between 4.2 and 300 K using a conventional four-probe method. The details of the procedure were described in our previous paper [14]. The samples have rectangular form

with typically a base 5 mm × 5 mm and a height 0.5 mm along the *c*-axis. The position of the voltage probe was 1–2 mm away from that of the current probe in the same basal plane. The voltage probes on both the basal planes were located on a straight line perpendicular to the basal plane. The current (typically 1–10 mA) was supplied through the current probes by a programmable current source (Keithley, model 224). The voltage generated across the voltage probes was measured by a digital nanovoltmeter (Keithley, model 181).

3. Results

3.1. Sample characterization

3.1.1. In-plane density. The stoichiometry (C_xSbCl_5) of the $SbCl_5$ GIC samples used here is listed in table 1. The value of x was determined from the weight-uptake measurement, where x is described by a product of a parameter s and stage number n. The reciprocal of the parameter s is proportional to the in-plane density of $SbCl_5$ in the intercalate layer. As listed in table 1 the value of s seems to depend on the stage number. Except for $s = 10.65$ for stage 2 and 13.69 for stage 9, the value of s is close to 12, as reported by Mélin and Hérold [22]. Our values of s are smaller than those reported by Homma and Clarke [17] ($s = 13.8$ for $n = 2$, 15.6 for $n = 4$, and 20.0 for $n = 5$). They have estimated the value of s from the $(00L)$ x-ray intensities under the assumption that there are only two molecular species ($SbCl_3$ and $SbCl_6^-$) in the intercalate layers. Their values of s may be overestimated because of neglecting the possibility of $SbCl_4^-$ and $SbCl_5$ species confirmed by Mössbauer [19, 20] and STEM [16].

Table 1. Characterization of $SbCl_5$ GICs used in the present work: stoichiometry (C_xSbCl_5) with $x = ns$ (n: stage number). The values of ρ_c at 290 K and *c*-axis repeat distance $I_c^{(n)}$ are also listed.

n	s	ρ_c (Ω cm)	$I_c^{(n)}$ (Å)
2	10.65	0.710	12.815 ± 0.006
3	12.69	1.0388	16.190 ± 0.015
4	12.16	1.375	19.584 ± 0.030
5	11.85	1.350	22.866 ± 0.024
6	11.40	1.075	25.737 ± 0.159
7	12.23	0.958	29.364 ± 0.142
9	13.69	0.760	36.370 ± 0.179
HOPG	—	0.0994	

3.1.2. Hendricks–Teller type stage disorder. A typical example of $(00L)$ x-ray scattering intensities against wave number Q_c at 295 K for the stage-5 $SbCl_5$ GIC sample is shown in figure 1. This result indicates that all the Bragg peaks are well indexed to stage-5 reflections with the *c*-axis repeat distance $I_c^{(5)} = 22.866 \pm 0.024$ Å. The values of *c*-axis repeat distance $I_c^{(n)}$ for each stage number are listed in table 1. For the stage-n $SbCl_5$ GIC ($n = 2, 3, 4$, and 5) we determined the peak position Q_c for each $(00L)$ Bragg reflection from the least-squares fit of the $(00L)$ Bragg peak to the theoretical curve expressed by a sum of Gaussian distribution and quadratic background. We find that the peak position of each $(00L)$ Bragg reflection for the stage-n $SbCl_5$ GIC slightly deviates from the average position $Q_L^{(n)} = (2\pi/I_c^{(n)})L$ of the pure stage-n $SbCl_5$ GIC. In figure 2 we show the L-dependence of the peak shift Δ_{PS} of the $(00L)$ Bragg reflection, from the average position

$Q_L^{(4)}$ of the pure stage 4, for stage-4 $SbCl_5$ GIC. The peak shift Δ_{PS} sinusoidally oscillates with the Bragg index L around $\Delta_{PS} = 0$, which is one of the important features for the Hendricks–Teller stage disorder [23]. When stage-$(n-2)$, $(n-1)$, (n), $(n+1)$, and $(n+2)$ packages with the probabilities of f_{n-2}, f_{n-1}, f_n, f_{n+1}, and f_{n+2} (f_n being much larger than f_{n-2}, f_{n-1}, f_{n+1}, and f_{n+2}) are randomly arranged along the c-axis, the peak shift $\Delta_{PS}^{(n)}(L)$ is predicted to be described by [23]

$$\Delta_{PS}^{(n)}(L) = \delta_n \left[\sin\left(\frac{2\pi d_G L}{I_c^{(n)}}\right) + \varepsilon_n \sin\left(\frac{4\pi d_G L}{I_G^{(n)}}\right)\right] \tag{1}$$

with $d_G = 3.35$ Å for the distance between nearest-neighbour graphite (G) layers without intervening intercalate (I) layer, $\delta_n = [f_{n-1} - f_{n+1}]/[f_n I_c^{(n)}]$, and $\varepsilon_n = (f_{n-2} - f_{n+2})/(f_{n-1} - f_{n+1})$. For stage-4 $SbCl_5$ GIC the data of Δ_{PS} against L (see figure 2) fall on the dotted line described by (1) with $\delta_4 = -0.015$ Å^{-1} and $\varepsilon_4 = 0.7$: $f_3 - f_5 = -0.29 f_4$ (< 0) and $f_2 - f_6 = -0.21 f_4$ (< 0). Similarly we obtain $\delta_2 = -0.004$ Å^{-1} and $\varepsilon_2 = 0.7$: $f_1 - f_3 = -0.051 f_2$ (< 0) and $f_4 = 0.036 f_2$ for stage 2, $\delta_3 = -0.006$ Å^{-1} and $\varepsilon_3 = 0.7$: $f_2 - f_4 = -0.097 f_3$ (< 0) and $f_1 - f_5 = -0.068 f_3$ (< 0) for stage 3, and $\delta_5 = 0.012$ Å^{-1} and $\varepsilon_5 = -0.7$: $f_4 - f_6 = 0.27 f_5$ (> 0) and $f_3 - f_7 = -0.19 f_5$ (< 0) for stage 5. The relatively large values of δ_n for stages 4 and 5 compared to those for stages 2 and 3 indicate that the degree of Hendricks–Teller stage disorder is high for stages 4 and 5. For the $(00L)$ x-ray diffraction patterns of stage-n $SbCl_5$ GICs ($n = 6$, 7, and 9) we find the Bragg reflections from $(n-1)$- and $(n+1)$-stages are superimposed on those from the n-stage, indicating that samples are ones with mixed stages.

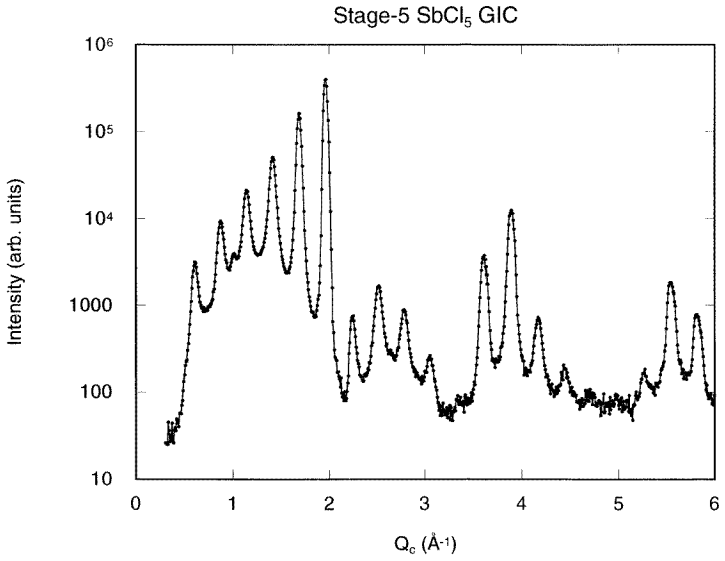

Figure 1. $(00L)$ x-ray scattering intensity against Q_c (Å^{-1}) at 295 K for the stage-5 $SbCl_5$ GIC.

In table 1 we show the average c-axis repeat distance $I_c^{(n)}$. Relatively large uncertainties in $I_c^{(n)}$ are partly due to the oscillations of Δ_{PS} with L for stages 4 and 5 and due to the mixed stages for stages 6, 7, and 9.

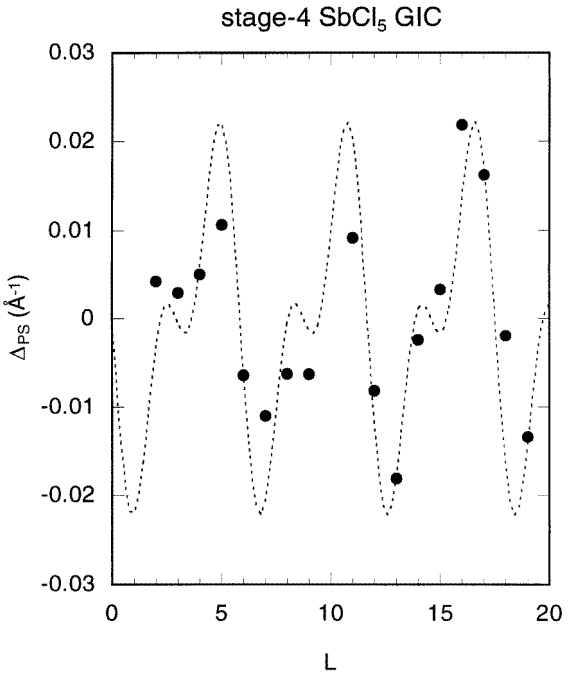

Figure 2. Peak shift Δ_{PS} of the $(00L)$ Bragg reflection from the average position $Q_L^{(4)} = (2\pi/I_c^{(4)})L$ for stage-4 $SbCl_5$ GIC as a function of L, where $I_c^{(4)}$ is the c-axis repeat distance and L is the Bragg index. The dotted line is denoted by (1) with $\delta_4 = -0.015$ Å^{-1} and $\varepsilon_4 = 0.7$.

3.2. ρ_c against T in the absence of H

3.2.1. ρ_c against stage number. In figure 3(a) we show a plot of ρ_c at 290 K (denoted by closed circles) as a function of stage number n for $SbCl_5$ GICs. For comparison we also show the plot of ρ_c (denoted by open circles) against n for $MoCl_5$ GICs [14], where HOPG materials used as graphite host for $MoCl_5$ GICs are the same as those for $SbCl_5$ GICs. The features of figure 3(a) are summarized as follows. (i) For $SbCl_5$ GIC the resistivity ρ_c has a maximum around stages 4 and 5, while for $MoCl_5$ GICs the resistivity ρ_c has a maximum around stages 3 and 4. (ii) The values of ρ_c for stage-2 and 3 $SbCl_5$ GICs are almost the same as those for $MoCl_5$ GICs with the same stage number, respectively, while the values of ρ_c for $SbCl_5$ GICs with $n \geqslant 4$ are much larger than those of $MoCl_5$ GICs with the same stage number n, respectively. (iii) The value of ρ_c with further increasing stage number tends to approach a value of ρ_c for HOPG (=0.0994 Ω cm). Note that our data of ρ_c against stage number do not agree well with those reported by Morelli and Uher [1]: (i) their values of ρ_c are relatively smaller than ours for the same stage number and (ii) their data of ρ_c against stage number seem to show a maximum near stage 3.

In figure 3(b) we show the stage dependence of ρ_c at 5 K for $SbCl_5$ GICs and $MoCl_5$ GICs. It is rather different from that at 290 K for the high-stage side. The value of ρ_c at 5 K for $SbCl_5$ GICs shows a local maximum at $n = 4$ and a local minimum at $n = 5$, and increases with further increasing stage number, while the value of ρ_c at 5 K for $MoCl_5$ GICs shows a local maximum at $n = 3$ and a local minimum at $n = 6$, and increases with further increasing stage number.

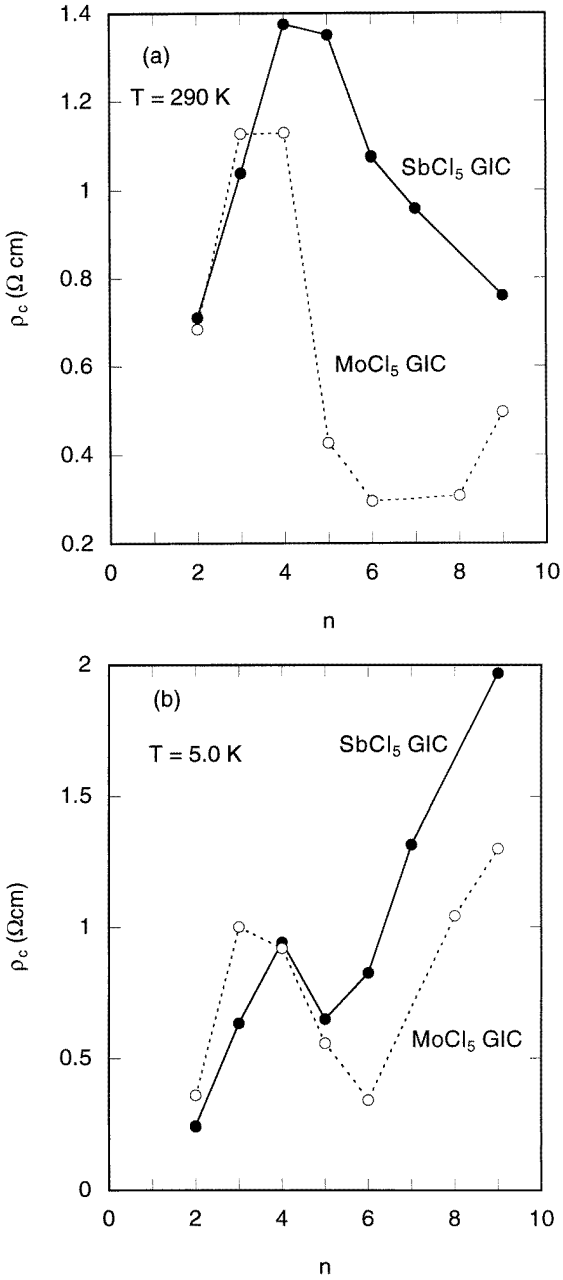

Figure 3. Stage number (n-) dependence of ρ_c for $SbCl_5$ GICs (●) and $MoCl_5$ GICs (○) [14] at (a) 290 K and (b) 5 K. Both GICs are based on HOPG of the same origin: $\rho_c = 0.0994\ \Omega$ cm at 290 K for HOPG.

3.2.2. Temperature dependence of ρ_c: thermal hysteresis. We have measured the c-axis resistivity ρ_c of $SbCl_5$ GICs as a function of temperature in the absence of an external magnetic field. The measurements were carried out as follows. First samples were cooled rather rapidly from RT to 4.2 K, typically at the rate of 0.3 K min^{-1} from RT to 170 K and

1.2 K min^{-1} from 170 to 4.2 K. The data of ρ_c against T obtained in this cooling process are defined as $\rho_c(T\downarrow)$. After keeping samples at 4.2 K for typically one hour, samples were heated slowly from 4.2 K to RT, typically at the rate of 0.08 K min^{-1}. The data of ρ_c against T obtained in this heating process are defined as $\rho_c(T\uparrow)$. We note that the value of $\rho_c(T\uparrow)$ at RT after the heating process coincides with that of $\rho_c(T\downarrow)$ at RT before the cooling process. The values of $\rho_c(T\downarrow)$ and $\rho_c(T\uparrow)$ are reproducible under the same conditions of cooling and heating processes.

Figure 4(a) shows the T-dependence of ρ_c for stage-2 $SbCl_5$ GIC. The resistivity ρ_c shows a metallic behaviour with monotonic increases of ρ_c with increasing temperature. The T-dependence of $\rho_c(T\uparrow)$ is well described by

$$\rho_c(T) = A + BT + CT^2 \tag{2}$$

with the coefficients $A = 0.2317\ \Omega$ cm, $B = 8.359 \times 10^{-4}\ \Omega$ cm K^{-1}, and $C = 2.423 \times 10^{-6}\ \Omega$ cm K^{-2}, for 20 K $\leqslant T \leqslant$ 300 K. The characteristic temperature $T_1 (= B/C)$ is estimated as 345 K, which is on the same order as that ($T_1 = 530$ K [14]) for stage-2 $MoCl_5$ GIC having a metallic behaviour. Figures 4(b) and (c) show the T-dependence of ρ_c for stage-3 and 4 $SbCl_5$ GICs, respectively, which is rather different from that for stage-2 $SbCl_5$ GIC. The resistivity $\rho_c(T\downarrow)$ monotonically decreases with decreasing temperature, showing a metallic behaviour, while $\rho_c(T\uparrow)$ has a very complicated T-dependence which includes local minima and maxima. Note that $\rho_c(T\uparrow)$ strongly depends on the heating rate of samples. As the heating rate is increased from 0.08 to 0.3 K min^{-1}, the difference between $\rho_c(T\downarrow)$ and $\rho_c(T\uparrow)$ becomes small in the temperature range between 180 and 250 K. The locations of temperatures for local maximum, local minimum, and change in $d\rho_c/dT$ do not depend on the heating rate. The details of this effect will be reported elsewhere [24]. Figures 4(d) and (e) show the T-dependence of ρ_c for stage-5 and 6 $SbCl_5$ GICs, respectively. The resistivity ρ_c decreases with increasing temperature and exhibits a local minimum at 48 K for stage 5 and 57 K for stage 6. The resistivity $\rho_c(T\uparrow)$ for stage 5 has a drastic change in $d\rho_c/dT$ at 243 K, while $\rho_c(T\uparrow)$ for stage 6 has local minima at 205.2 and 229.0 K. Figures 4(f) and (g) show the T-dependence of ρ_c for stage-7 and 9 $SbCl_5$ GICs, respectively. For both stages ρ_c shows a semiconductor-like behaviour at low temperatures, undergoing a crossover to the metallic behaviour at high temperatures. We note the result of $\rho_c(T\uparrow)$ for stage-8 $SbCl_5$ GIC reported by Andersson *et al* [8]: local minima at 203 and 232 K and a local maximum at 220 K.

3.2.3. Logarithmic behaviour of ρ_c at low temperatures. Here we discuss the T-dependence of ρ_c for stage-5 and 6 $SbCl_5$ GICs at low temperatures. In figures 5(a) and (b) we show the plots of ρ_c against $\log_{10}(T)$ for stage-5 and 6 $SbCl_5$ GICs, respectively. The resistivity ρ_c increases with decreasing temperature at low temperatures and reaches a saturated value below 10 K. These data for stage-5 and 6 $SbCl_5$ GICs are fitted to a straight line described by

$$\rho_c(T) = a - b\ln(T) \tag{3}$$

in a limited temperature range where no saturation of ρ_c occurs. The least-squares fit of the data to (3) yields the constants a and b: $a = 0.6842\ \Omega$ cm and $b = 5.313 \times 10^{-3}\ \Omega$ cm in stage 5 for 16.5 K $\leqslant T \leqslant$ 26 K, $a = 0.843\ \Omega$ cm and $b = 7.551 \times 10^{-3}\ \Omega$ cm in stage 6 for 18 K $\leqslant T \leqslant$ 26 K. Similar logarithmic behaviour is observed in ρ_c for stage-3 and 4 $MoCl_5$ GICs: $a = 1.005\ \Omega$ cm, $b = 2.439 \times 10^{-3}\ \Omega$ cm for stage 3 and $a = 0.923\ \Omega$ cm and $b = 2.645 \times 10^{-3}\ \Omega$ cm for stage 4. In contrast to ρ_c for stage-5 and 6 $SbCl_5$ GICs, ρ_c of stage-3 and 4 $MoCl_5$ GICs shows a logarithmic behaviour even at 5 K without saturation.

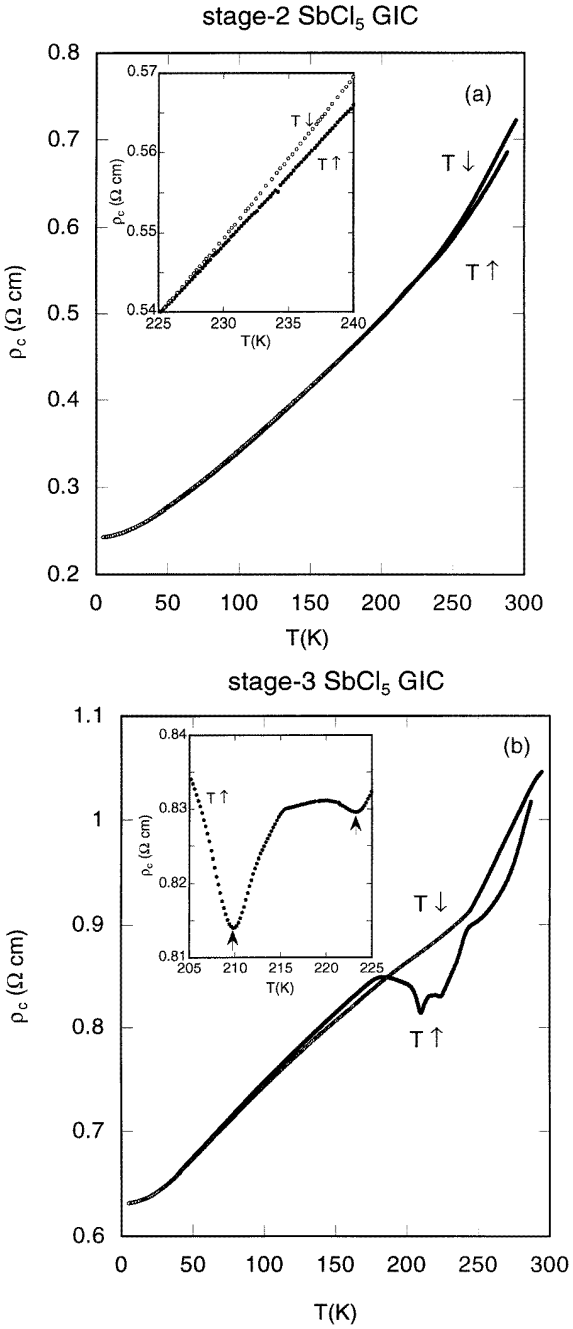

Figure 4. ρ_c against T for stage- (a) 2, (b) 3, (c) 4, (d) 5, (e) 6, (f) 7, and (g) 9 $SbCl_5$ GICs measured during the cooling and heating processes described in the text. The details of $\rho_c(T\uparrow)$ against T for $190 \leqslant T \leqslant 240$ K are shown in the inset.

The saturation effect of ρ_c observed in stage-5 and 6 $SbCl_5$ GICs may suggest another possibility that rather than the logarithmic T-dependence, ρ_c of stage-5 and 6 $SbCl_5$ GICs can be expressed by a power law form ($\rho_c = a' - b'T^{p/2}$) over a wide temperature range $5\ \text{K} \leqslant T \leqslant 20$ K. This power law form is predicted for systems having an isotropic

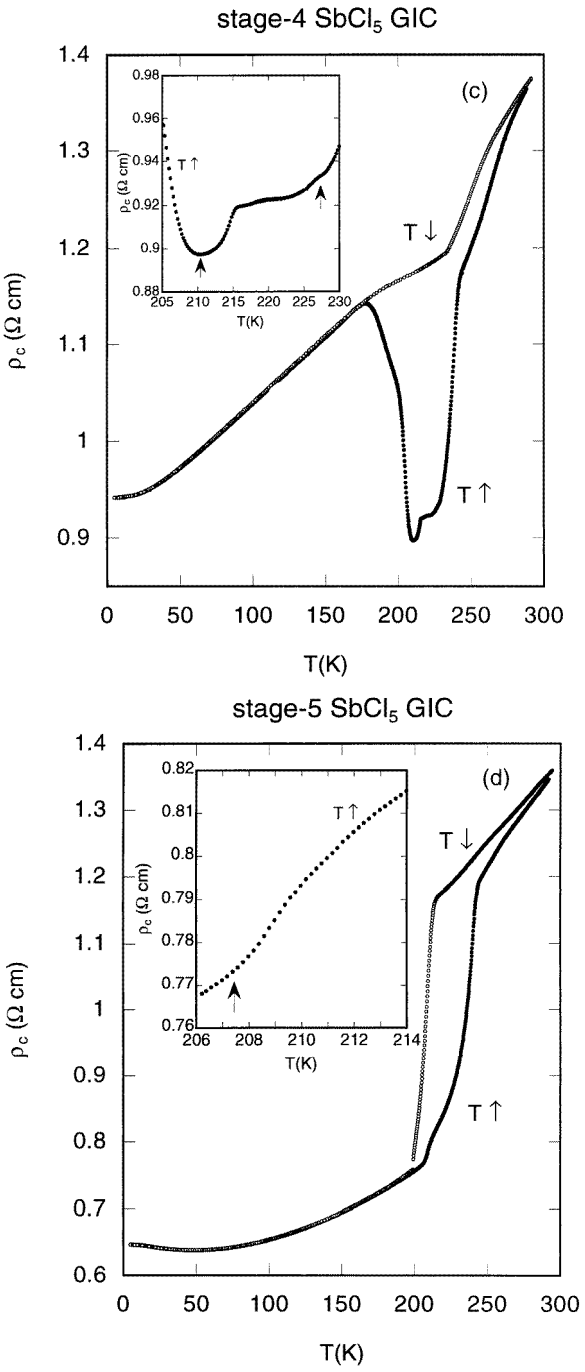

Figure 4. (Continued)

3D localization effect [25]. We find that the data of ρ_c against T are well fitted to the power law form with $a' = 0.671\ \Omega$ cm, $b' = 9.27 \times 10^{-7}$, and $p = 5.35$ for stage 5 and $a' = 0.825\ \Omega$ cm, $b' = 1.12 \times 10^{-5}$, and $p = 3.94$ for stage 6. These values of p are much

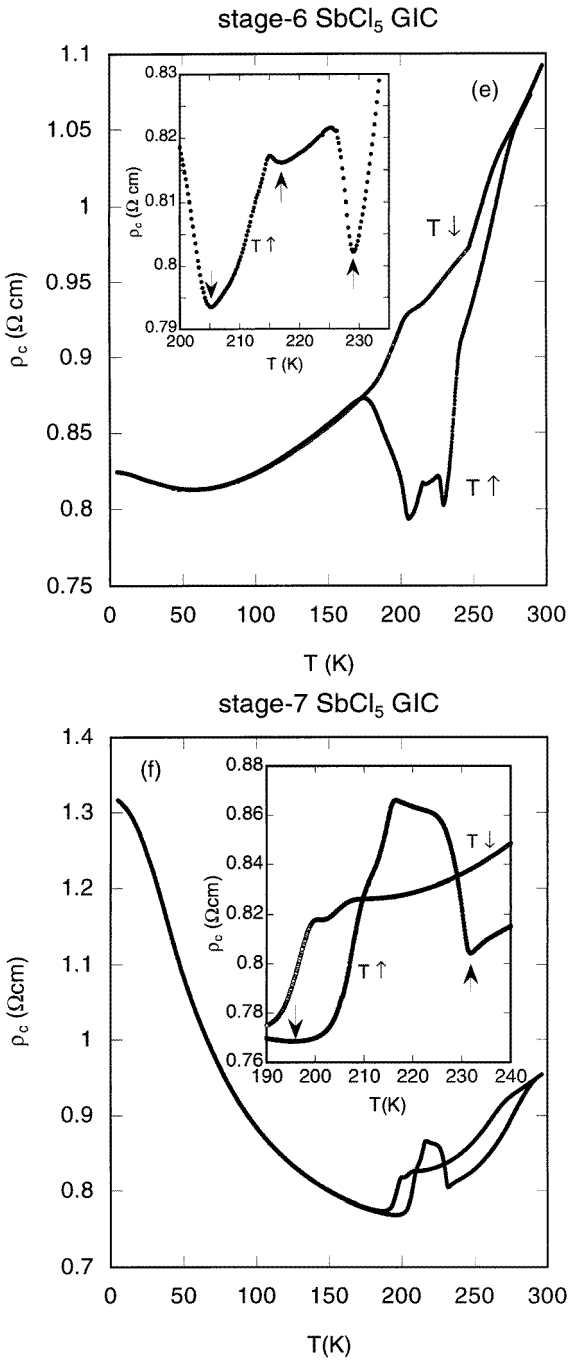

Figure 4. (Continued)

larger than those predicted from theories ($p = 1$–2) [25]. This result may suggest that the T-dependence of ρ_c cannot be explained in terms of the isotropic 3D localization effect. In spite of (i) the saturation of ρ_c at low temperatures and (ii) logarithmic T-dependence in an

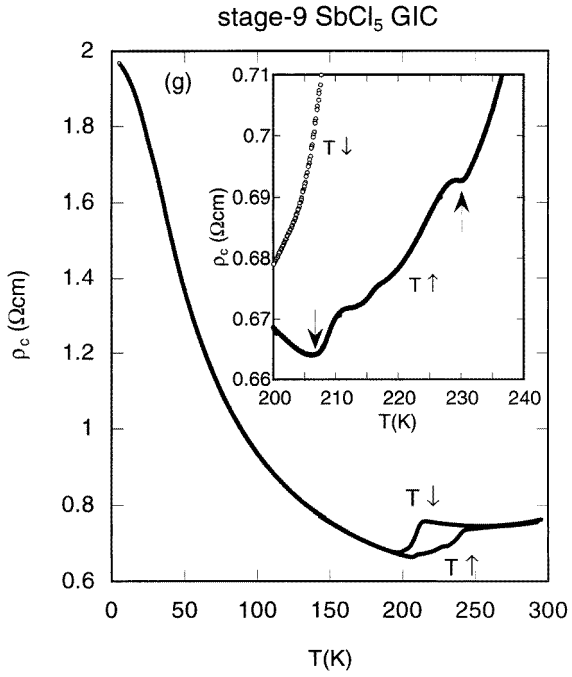

Figure 4. (Continued)

extremely limited temperature range, it may be concluded that ρ_c of stage-5 and 6 $SbCl_5$ GICs shows a logarithmic behaviour at low temperatures. Note that such a logarithmic behaviour has not been observed in the in-plane resistivity ρ_a at low temperatures for stage-2–6 $SbCl_5$ GICs and $MoCl_5$ GICs: it shows a metallic behaviour.

In the previous paper [14] it is concluded that the logarithmic behaviour in $MoCl_5$ GICs is attributed to either the 2D weak localization effect or the Kondo effect. Unlike Mo^{5+} with spin $S = 1/2$ in $MoCl_5$ GICs Sb atoms have no spin, implying no exchange interaction between Sb atoms and spins of π electrons. Thus the possibility of the Kondo effect may be ruled out for the logarithmic behaviour observed in $SbCl_5$ GICs.

3.3. Longitudinal magnetoresistance with H along the c-axis

3.3.1. Field dependence of $\Delta\rho_c/\rho_0$. In figure 6 we show the field (H) dependence of ρ_c for stage-3 to 6 $SbCl_5$ GICs with T varied as a parameter when an external magnetic field is applied along the c-axis (0 kOe $\leqslant H \leqslant$ 7 kOe). Figure 6(a) shows the H-dependence of $\Delta\rho_c/\rho_0$ for stage 3 $SbCl_5$ GIC at 4.74 K $\leqslant T \leqslant$ 13.97 K, where $\rho_0 = \rho_c(H = 0, T)$ and $\Delta\rho_c = \rho_c(H, T) - \rho_0$. The sign of $\Delta\rho_c/\rho_0$ is negative for 0 kOe $\leqslant H <$ 1 kOe and positive for 1 kOe $< H \leqslant$ 7 kOe. The resistivity $\Delta\rho_c/\rho_0$ has a negative local minimum ($= -1.5 \times 10^{-3}$) around 0.4 kOe and increases with further increasing field. Figure 6(b) shows the H-dependence of $\Delta\rho_c/\rho_0$ for stage-4 $SbCl_5$ GIC at $T =$ 4.18 and 10.17 K. The sign of $\Delta\rho_c/\rho_0$ is negative for 0 kOe $\leqslant H <$ 0.6 kOe and positive for 0.6 kOe $< H \leqslant$ 7 kOe. The resistivity $\Delta\rho_c/\rho_0$ has a negative local minimum ($= -1.5 \times 10^{-4}$) around 0.4 kOe and increases with further increasing field. Figure 6(c) shows the H-dependence of $\Delta\rho_c/\rho_0$ for stage-5 $SbCl_5$ GIC at $T =$ 4.29, 7.97,

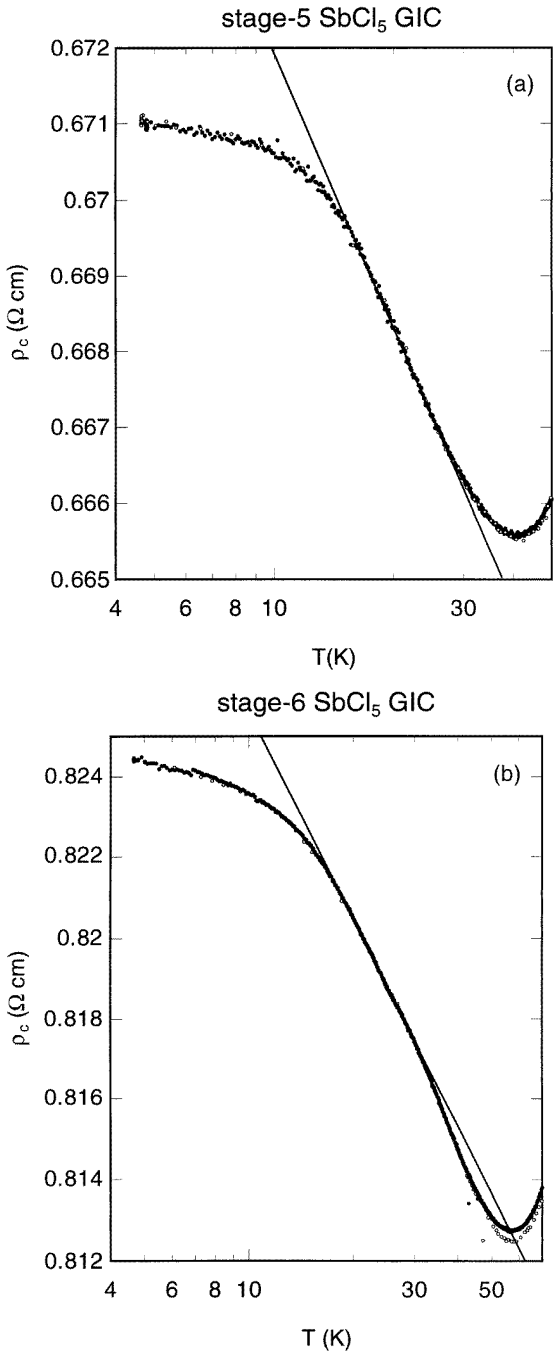

Figure 5. Plot of ρ_c as a function of $\log_{10}(T)$ for stage- (a) 5 and (b) 6 $SbCl_5$ GICs at low temperatures. The straight lines are described by (3) with a logarithmic behaviour in ρ_c.

and 65.9 K. The sign of $\Delta\rho_c/\rho_0$ is negative for 0 kOe $\leqslant H <$ 0.8 kOe and positive for 0.8 kOe $< H \leqslant$ 7 kOe. The resistivity $\Delta\rho_c/\rho_0$ has a negative local minimum ($= -1.5 \times 10^{-4}$) around 0.5 kOe and increases with further increasing field. Figure 6(d)

shows the H-dependence of $\Delta\rho_c/\rho_0$ for stage-6 $SbCl_5$ GIC at $T = 4.74$ K. The sign of $\Delta\rho_c/\rho_0$ is negative for 0 kOe $\leqslant H <$ 0.5 kOe and positive for 0.5 kOe $< H \leqslant 7$ kOe. The resistivity $\Delta\rho_c/\rho_0$ has a negative local minimum ($= -1.4 \times 10^{-4}$) around 0.25 kOe and increases with further increasing field. For stage-2 and 9 $SbCl_5$ GICs the resistivity $\Delta\rho_c/\rho_0$ at $T = 4.2$ K shows a positive MR for 0 kOe $\leqslant H \leqslant 7$ kOe. It almost linearly increases with increasing H. For stage-7 $SbCl_5$ GIC the sign of $\Delta\rho_c/\rho_0$ at 4.2 K is negative for 0 kOe $\leqslant H <$ 0.3 kOe and positive for 0.3 kOe $< H \leqslant 7$ kOe.

In summary, the resistivity $\Delta\rho_c/\rho_0$ shows a negative MR at low fields and a positive MR at higher fields for stage-3 to 7 $SbCl_5$ GICs, except for stage-2 and 9 $SbCl_5$ GICs with a positive MR for any fields. Similar behaviours of negative MR in $\Delta\rho_c/\rho_0$ were also observed in stage-4 and 5 $MoCl_5$ GICs: for both GICs the resistivity $\Delta\rho_c/\rho_0$ around 4.2 K shows a negative MR with a local minimum ($= -0.01$) around 2.5 kOe. In contrast with that of $SbCl_5$ GICs the negative MR effect is much more pronounced for $MoCl_5$ GICs.

3.3.2. T-dependence of $\Delta\rho_c/\rho_0$. In the insets of figure 6 we show the T-dependence of $\Delta\rho_c/\rho_0$ for stage-3 to 6 $SbCl_5$ GICs at various fixed fields ($H = 1.24$, 2.48, 3.69, 4.88, 5.97, and 6.82 kOe) in the temperature range between 4.2 and 300 K. For stage-2 and 3 $SbCl_5$ GICs the resistivity $\Delta\rho_c/\rho_0$, whose sign is positive at any temperature, monotonically decreases with increasing temperature. The T-dependence of $\Delta\rho_c/\rho_0$ for stage-4 $SbCl_5$ GIC is similar to that for stage-2 and 3 $SbCl_5$ GICs except for the temperature range 200 K $\leqslant T \leqslant$ 240 K. In this temperature region $\Delta\rho_c/\rho_0$ in particular at $H = 6.82$ kOe shows a local minimum around 210 K. Similar behaviour is also observed at $H = 6.82$ kOe for stage-5 and 6 $SbCl_5$ GICs. We note that the sign of $\Delta\rho_c/\rho_0$ at $H = 1.24$ kOe for stage-5 $SbCl_5$ GIC is slightly negative around 48 K where the resistivity $\rho_c(T)$ for $H = 0$ shows a local minimum. The T-dependence of $\Delta\rho_c/\rho_0$ for stage-7 and 9 $SbCl_5$ GICs is similar to that for stage-2 and 3 $SbCl_5$ GICs: (i) a positive sign of $\Delta\rho_c/\rho_0$ and (ii) a monotonic decrease of $\Delta\rho_c/\rho_0$ with increasing temperature.

Figure 7 shows the plot of $\Delta\rho_c/\rho_0$ at $T = 4.2$ K and $H = 6.82$ kOe for $SbCl_5$ GICs as a function of stage number. For comparison we also show the plot of $\Delta\rho_c/\rho_0$ at $T = 4.2$ K and $H = 6.82$ kOe for $MoCl_5$ GICs. The value of $\Delta\rho_c/\rho_0$ shows a minimum around $n = 5$ for both $SbCl_5$ and $MoCl_5$ GICs. The magnitude of $\Delta\rho_c/\rho_0$ for $SbCl_5$ GICs is roughly two times larger than that for $MoCl_5$ GICs for the same stage number.

4. Discussion

4.1. Phase transitions

According to the x-ray studies by Homma and Clarke [17], the stage-1 $SbCl_5$ GIC shows a partial 3D stacking coherence along the c-axis. For $n = 2$ the interplanar interaction between adjacent intercalate layers is weaker than that for $n = 1$. No structural change occurs on lowering temperature. This is consistent with our result that ρ_c for $n = 2$ shows no anomaly at any temperatures below RT. For higher stages ($n \geqslant 3$) there is no appreciable 3D structural correlation. This lack of 3D structural correlation for $n \geqslant 3$ persists at low temperatures. The molecular species are in either completely disordered states or partially disordered states at RT, and undergo a first-order phase transition into the low-temperature ordered state.

The incomplete disproportionation occurring in the intercalate layers during the intercalation process gives rise to molecular species of $SbCl_3$, $SbCl_4^-$, $SbCl_5$, and $SbCl_6^-$ [15–20]. The $SbCl_6^-$ species forms a commensurate structure of $(\sqrt{7} \times \sqrt{7})$R(19.1°) with

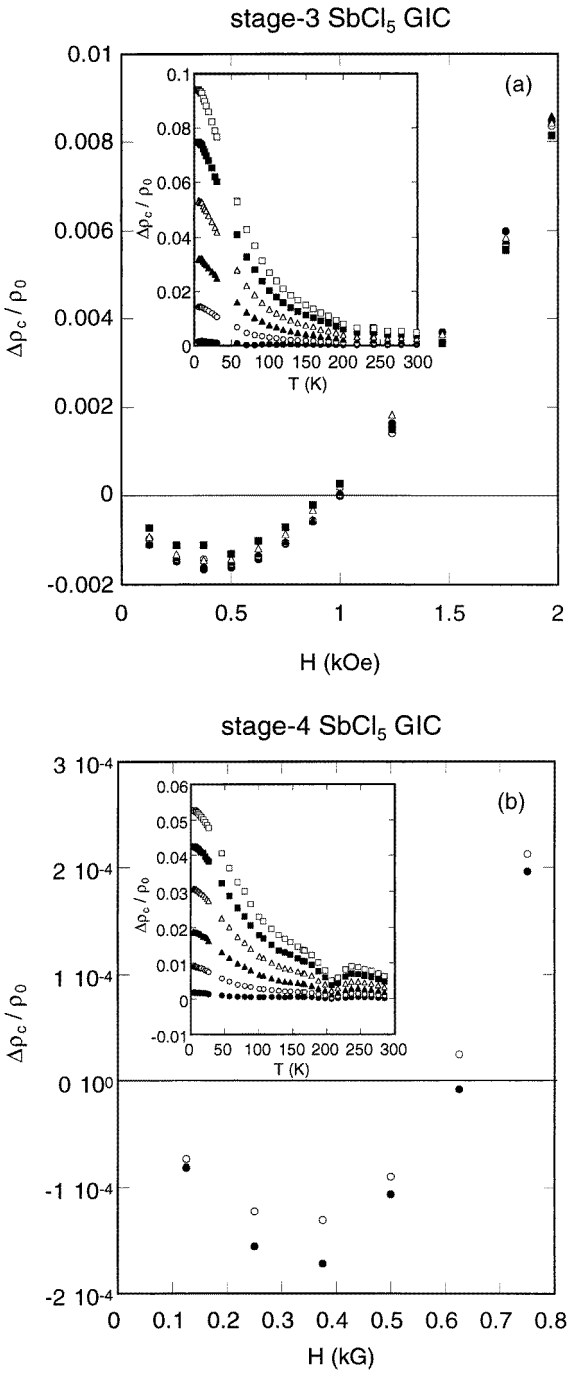

Figure 6. H-dependence of $\Delta\rho_c/\rho_0$ for stage- (a) 3, (b) 4, (c) 5, and (d) 6 $SbCl_5$ GICs. (a) $T = 4.74$ K (●), 6.06 K (○), 8.07 K (▲), 10.26 K (△), 13.97 K (■), and 131.76 K (□); (b) $T = 4.18$ K (●) and 10.17 K (○); (c) 4.29 K (●), 7.97 K (○), and 65.9 K (▲), and (d) $T = 4.74$ K (●). $\rho_c(T, H)$ is the c-axis resistivity at T in the presence of an external field H along the c-axis, $\Delta\rho_c = \rho_c(T, H) - \rho_c(T, H = 0)$, and $\rho_0 = \rho_c(T, H = 0)$. In the inset the T-dependence of $\Delta\rho_c/\rho_0$ for stage- (a) 3, (b) 4, (c) 5, and (d) 6 $SbCl_5$ GICs is also shown, where $H = 1.24$ (●), 2.48 (○), 3.69 (▲), 4.88 (△), 5.97 (■), and 6.82 kOe (□).

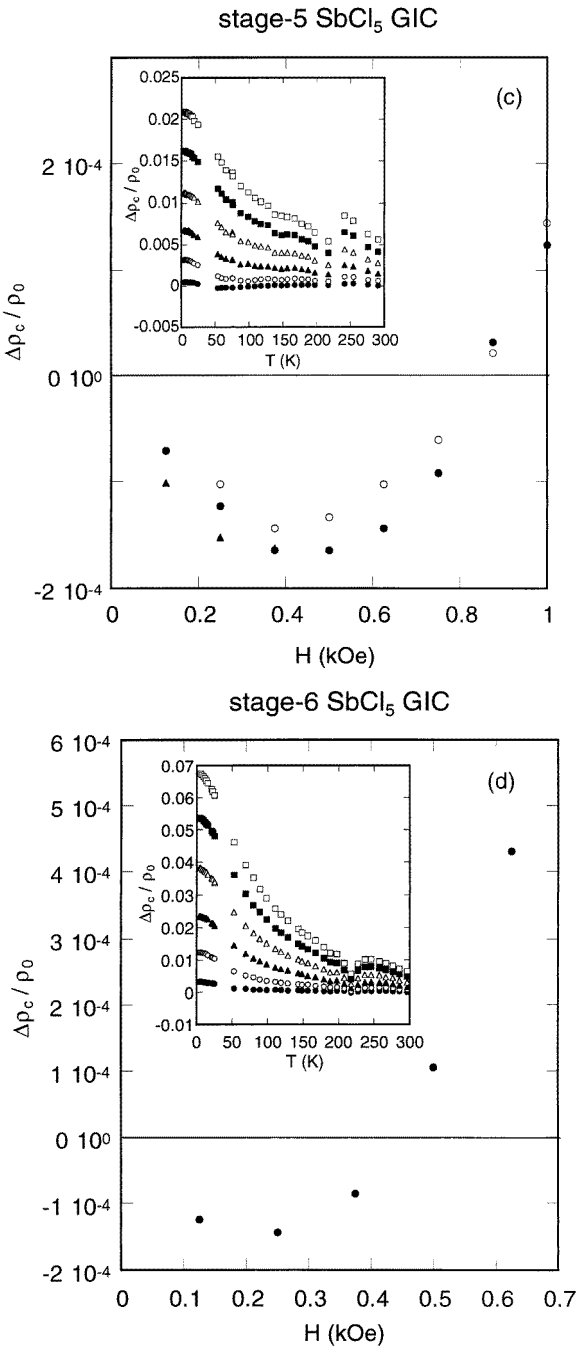

Figure 6. (Continued)

one $SbCl_6^-$ molecule per $\sqrt{7}\times\sqrt{7}$ unit cell (see figure 8(a)), which is stable up to at least RT for any stage n. The $SbCl_3$ species forms a commensurate structure of $(\sqrt{39}\times\sqrt{39})$R(16.1°) having p (integer) $SbCl_3$ molecules per $\sqrt{39}\times\sqrt{39}$ unit cell. In figure 8(b) we show the in-plane structure model for $p = 4$ which can be derived from discussions based on the in-plane

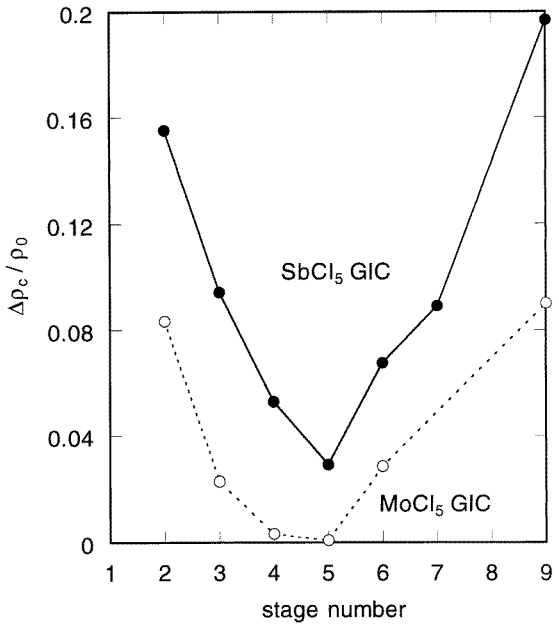

Figure 7. Plot of $\Delta\rho_c/\rho_0$ at $T = 4.2$ K and $H = 6.82$ kOe as a function of stage number for $SbCl_5$ GICs (●) and $MoCl_5$ GICs (○).

density ($s = 12$) and the structure of pristine $SbCl_3$ [26]. This structure model is different from that proposed by Homma and Clarke [17] (for example $s = 15.6$ for $n = 4$). In the intercalate layer $SbCl_3$ molecular species form two kinds of trigonal prism: one Sb atom and three Cl atoms located in a trigonal plane below the Sb atom, and another Sb atom and three Cl atoms located in a trigonal plane above the Sb atom. The energy of this molecule is the same for the two possible positions of the Sb atoms. It is well known that the pristine $SbCl_3$ molecule has a rather large electric dipole moment $\mu = 3.9\ D$ ($D = 10^{-18}$ esu cm) [27] with its direction pointing away from the Sb atom and perpendicular to the plane of the Cl atoms. In figure 8(b) we show possible directions of electric dipole moments which are either parallel or antiparallel to the c-axis. This dipole moment $\boldsymbol{\mu}_1$ is assumed to be coupled with the nearest-neighbour one $\boldsymbol{\mu}_2$ through a dipole–dipole interaction

$$U_{12} = \frac{R_{12}^2(\boldsymbol{\mu}_1 \cdot \boldsymbol{\mu}_2) - 3(\boldsymbol{\mu}_1 \cdot \boldsymbol{R}_{12})(\boldsymbol{\mu}_2 \cdot \boldsymbol{R}_{12})}{R_{12}^5} \tag{4}$$

where $\boldsymbol{R}_{12}$ is a position vector connecting between the locations of $\boldsymbol{\mu}_1$ and $\boldsymbol{\mu}_2$. When both $\boldsymbol{\mu}_1$ and $\boldsymbol{\mu}_2$ are perpendicular to the position vector $\boldsymbol{R}_{12}$, this interaction favours a configuration of dipole moments with the direction of $\boldsymbol{\mu}_1$ being antiparallel to that of $\boldsymbol{\mu}_2$.

The distance between nearest-neighbour electric dipoles is given by $|\boldsymbol{R}_{12}|(= 7.64$ Å), which is of the order of diameter of pristine $SbCl_3$ molecules [26]. Then the dipole–dipole interaction U_{12} can be estimated as 3.41×10^{-14} erg, where $T_{12} = U_{12}/k_B = 244$ K, which is close to the critical temperature T_{cu} (=223–231 K) as will be defined later.

This dipole–dipole interaction favours an antiparallel configuration for the nearest-neighbour $SbCl_3$ molecules. For nearest-neighbour interactions there are four antiparallel couplings and two parallel couplings. This is also true for next-nearest-neighbour interactions. The competition between these interactions may give rise to a frustration effect inside the system. This situation is similar to that of the 2D Ising antiferromagnet

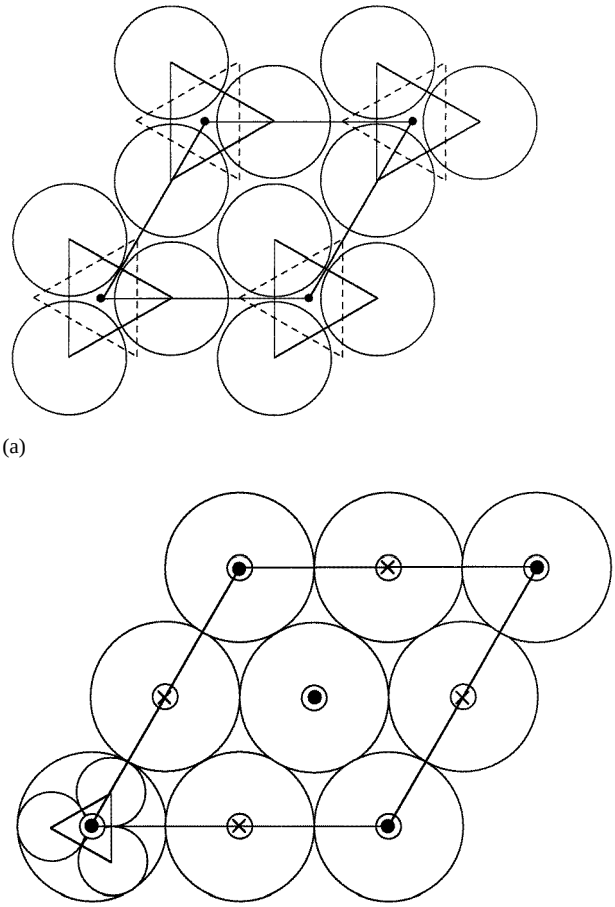

Figure 8. (a) A possible in-plane configuration of $SbCl_6^-$ molecules forming a $(\sqrt{7} \times \sqrt{7})R(19.1^\circ)$ structure: Sb atoms denoted by closed circles and Cl ions in the upper Cl layers denoted by open circles. The radius of the Cl^- ion is 1.80 Å. (b) A possible in-plane configuration of $SbCl_3$ molecules for the close packing of four molecules into a unit cell of $\sqrt{39} \times \sqrt{39}$. The electric dipole moments of $SbCl_3$ have two possible directions: one is directed into the plane of graphite layer and the other out of this plane. The radius of $SbCl_3$ molecules is 3.82 Å.

on the triangular lattice with spin frustration effects arising from competing intraplanar exchange interactions.

In the previous paper [14] we have shown that the resistivity ρ_c(GIG) associated with the carrier transfer across the G–I–G sandwich layer is described as

$$\rho_c(\mathrm{GIG}) = \frac{\hbar^3}{16e^2 d_I m^*} \left(\frac{N}{N_I}\right) \frac{\Gamma}{V_0^2} \tag{5}$$

where d_I is the thickness of GIG sandwich layers, V_0 is the matrix element of the scattering potential, N_I is the number of conduction paths (conduction channels), N is the number of unit cells, m^* is the effective mass of carriers, and $\Gamma/\hbar$ is the relaxation rate of carriers in the graphite basal plane. $\Gamma/\hbar$ is a sum of the relaxation rates due to phonon and impurity

scattering: $\Gamma = \Gamma^{(e-p)} + \Gamma^{(I)}$. It should be noted that in (5) the resistivity decreases with increasing V_0^2. This is in contrast with the in-plane resistivity which increases with the magnitude of scattering potential in the intercalate layer. When the effect of the dipole moments of $SbCl_3$ molecules on the c-axis conduction is taken into account, V_0^2 may be replaced by $V_0^2 + V_d^2$, where V_d^2 is proportional to the fluctuation of dipole moments. It is expected that this fluctuation becomes large on approaching a critical temperature. According to (5) the c-axis resistivity is inversely proportional to the square of the matrix element of the scattering potential. As the fluctuation becomes large the square of the matrix element becomes large, leading to a local minimum of ρ_c at the critical temperature. In contrast to the c-axis resistivity, the in-plane resistivity is predicted to be proportional to the square of the matrix element of the scattering potential, which leads to a local maximum at the critical temperature.

Here we define a critical temperature of $SbCl_5$ GICs by a temperature where $\rho_c(T\uparrow)$ has such local minima and changes in $d\rho_c/dT$ as denoted by arrows in figure 4. Figure 9 shows the stage dependence of critical temperatures thus obtained, where the data for stage 8 obtained by Andersson *et al* [8] are also included. The critical temperatures are divided into the following two according to their characteristics: $T_{cl} = 196$–211 K and $T_{cu} = 223$–231 K. The value of T_{cl} tends to decrease with increasing stage number ($3 \leqslant n \leqslant 7$) and that (ii) the value of T_{cu} is less weakly dependent on the stage number ($3 \leqslant n \leqslant 9$). Note that a slight increase in T_{cl} around $n = 8$–9 may be related to the fact that these samples are formed of mixed stages as pointed out in section 3.1.2. Then the above result may suggest that the 2D and 3D long-range dipole orders appear at T_{cu} and T_{cl}, respectively. Well above T_{cu} the system of $SbCl_3$ molecules is in a structurally disordered state. The 2D structural correlation length drastically increases on approaching T_{cu} from the high-temperature side, giving rise to the enhancement of intraplanar correlation between dipoles of $SbCl_3$ molecules in each $SbCl_5$ layer. A 2D long-range dipole order is established below T_{cu}. The effective interplanar interaction between dipoles of $SbCl_3$ is a driving force for the 3D ordering process of dipoles. The interaction may be determined by a product of very weak interplanar interaction between dipoles and a square of intraplanar dipole correlation length, in analogy with effective interplanar interactions between spins in stage-2 $CoCl_2$ GIC [28]. The growth of the intraplanar dipole correlation length is limited by the size of $SbCl_3$ forming islands in the $SbCl_5$ layer [17]. A 3D long-range dipole order appears below T_{cl} a little lower than T_{cu} because of the suppression of divergence in the effective interplanar interactions between dipoles around T_{cu}. We note that the c-axis conduction mechanism near T_{cu} and T_{cl} is not well understood.

4.2. Logarithmic behaviour of c-axis resistivity

In the c-axis electrical conduction in GICs carriers mostly experience diffusive motions in the graphite layers and occasionally jump to the nearest-neighbour graphite layers. The total c-axis resistivity ρ_c is formed of a series connection of c-axis resistivities from G–I–G and G–G [14]. The c-axis resistivity ρ_c(GIG) is proportional to the in-plane resistivity of the bounding G layer next to the I layer. The c-axis resistivity ρ_c(GG) between two G layers with no intervening I layer is proportional to the in-plane resistivity of the interior G layers. In acceptor GICs the charge transfers occur from each graphite layer to the intercalate layer during the intercalation process. The amount of charge transfer between the interior G layers and I layers is much smaller than that between the bounding G layers and I layers, implying the small density of states in the interior G layers. When this density of states is sufficiently small, ρ_c(GG) in the interior G layers becomes a bottleneck in ρ_c [29]. At

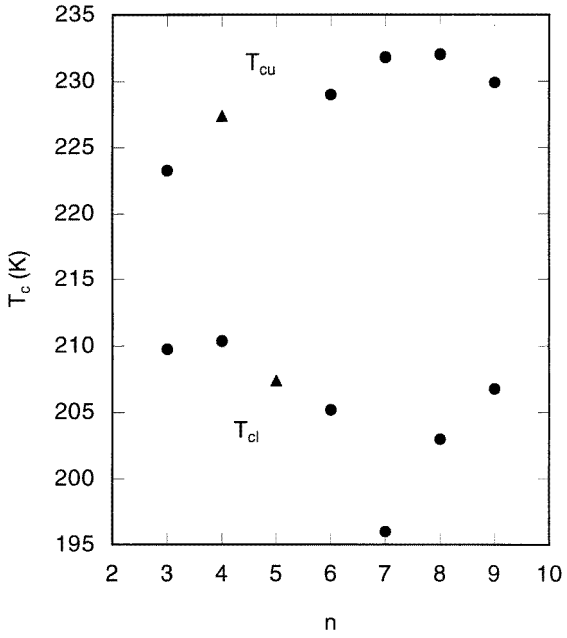

Figure 9. Stage dependence of critical temperatures T_{cl} and T_{cu} for $SbCl_5$ GICs, where $\rho_c(T\uparrow)$ has local minima (●) and changes in $d\rho_c/dT$ (▲) as denoted by arrows in figure 4. The data of stage 8 [8] are also included.

high temperatures it has a metallic T-dependence for low stages and a semiconductor-like dependence for high stages.

Here we discuss the logarithmic behaviour in ρ_c at low temperatures observed in $SbCl_5$ GICs ($n = 5$ and 6) as well as $MoCl_5$ GICs ($n = 3$ and 4). To this end first we assume that the 2D weak localization effect occurs in both the bounding and interior G layers due to the quantum interference of the carriers on impurities and defects. The in-plane conductivity due to the localization effect can be described by [25, 30–33]

$$\sigma_a(\mathrm{T}) = \sigma_B - \frac{e^2}{2\pi^2\hbar}\ln\left(\frac{L_\varepsilon}{L_0}\right)^2 \tag{6}$$

where L_k is the diffusion length defined by $L_k = (D\tau_k)^{1/2}$ for $k = 0$ for the elastic scattering and $k = \varepsilon$ for the inelastic scattering, D is the 2D diffusion constant, τ_k is a relaxation time, and σ_B is the Boltzmann (normal) conductivity proportional to L_0. If $\tau_\varepsilon \approx T^{-p}$ (p: an exponent) and the Boltzmann term σ_B is much larger than the correction term, the in-plane resistivity is described by the form $\rho_a = \rho_1 - \rho_0 \ln(T)$, where ρ_0 and ρ_1 are constant resistivities. Then the c-axis resistivity also shows a logarithmic behaviour associated with the in-plane resistivity of the corresponding G layer. Because of small density of states in the interior G layers, the mean free path l_ε for the inelastic scattering is relatively long, which also means a long L_ε, where $L_\varepsilon = (l_0 l_\varepsilon/2)^{1/2}$ and l_0 is the mean free path for the elastic scattering. On the other hand, the large amount of charge transfer between the bounding G layers and I layers leads to a relatively short L_ε. According to (6) this implies that the 2D weak localization effect occurs mainly in the interior G layers. The logarithmic behaviour in ρ_c arises from the in-plane resistivity of the interior G layers. This prediction is consistent with the fact that the logarithmic behaviour in ρ_c is observed only in high-

stage GICs having interior G layers [14]. Here we note that the stage number where the logarithmic behaviour of ρ_c appears almost coincides with that where ρ_c at RT against n shows a local maximum: $n = 4$–5 for $SbCl_5$ GICs and $n = 3$–4 for $MoCl_5$ GICs (see figure 3(a)). This may suggest that the main contribution to the high value of ρ_c at RT arises from the interior graphite layers with smaller charge transfer.

The situation is very different for the in-plane resistivity. The total in-plane resistivity ρ_a consists of a parallel connection of in-plane resistivity from each G layer. The resistivity ρ_a is dominantly determined by the in-plane resistivity from the bounding G layers which has no logarithmic behaviour. This prediction is consistent with our experimental results: no logarithmic behaviour is observed in the in-plane resistivity of stage-2–6 $MoCl_5$ GICs and stage-2–6 $SbCl_5$ GICs.

4.3. Longitudinal negative magnetoresistance

We have found that high-stage $SbCl_5$ GICs ($n = 3$–7) as well as $MoCl_5$ GICs ($n = 4$–6) show a negative longitudinal MR at low magnetic fields, where the absolute value of $\Delta\rho_c/\rho_0$ at 4.2 K for $SbCl_5$ GICs is much smaller than that for $MoCl_5$ GICs: for $SbCl_5$ GICs $\Delta\rho_c/\rho_0 = -1.65 \times 10^{-3}$ for $n = 3$, -1.70×10^{-4} for $n = 4$ and 5, and -1.44×10^{-4} for $n = 6$, and $\Delta\rho_c/\rho_0 = -1 \times 10^{-2}$ for stage-4 to 6 $MoCl_5$ GICs. In order to explain these phenomena, here we assume again that a 2D weak localization effect occurs both in the bounding and interior layers of these GICs. A uniform magnetic field H which is applied along the c-axis weakens the localization effect [25, 30–33]. If the spin–orbit scattering and scattering by magnetic impurities are neglected, the relative resistivity in the presence of H for bounding and interior G layers can be given by the form

$$-\frac{\Delta\sigma_i}{\sigma_i} = -\frac{\Delta\sigma_B}{\sigma_B} + \frac{e^2}{2\pi^2\hbar d_i\sigma_B}\Gamma(L_0, L_\varepsilon, L_H) \tag{7}$$

with

$$\Gamma(L_0, L_\varepsilon, L_H) = \Psi\left[\frac{1}{2} + \left(\frac{L_H}{L_0}\right)^2\right] - \Psi\left[\frac{1}{2} + \left(\frac{L_H}{L_\varepsilon}\right)^2\right] - \ln\left(\frac{L_\varepsilon}{L_0}\right)^2 \tag{8}$$

for $L_0^2 \ll L_H^2$, L_ε^2, where $i =$ GG and GIG, $d_i = d_I$ for GIG and d_G for GG and $\Psi(x)$ is the digamma function which has the limiting forms $\Psi(1/2 + x) = \ln(x) + 1/24x^2$ for $x \gg 1$ and -1.9635 for $x = 0$. The first term of (7), called the Boltzmann term, is positive. The magnetic length L_H is defined by $L_H = (\hbar c/4eH)^{1/2}$. For the interior G layers ($i =$ GG) with $L_H^2 \ll L_\varepsilon^2$, the function Γ can be approximated as

$$\Gamma(L_0, L_\varepsilon, L_H) \approx -\ln\left(\frac{L_\varepsilon}{L_H}\right)^2 = -\ln\left(\frac{4eL_\varepsilon^2}{\hbar c}H\right) \tag{9}$$

which is negative. The sign of the MR is determined by a balance between the positive Boltzmann term and the negative second term in (7). For the bounding layers ($i =$ GIG) with $L_0^2 \ll L_\varepsilon^2 \ll L_H^2$, on the other hand, the function Γ can be approximated as

$$\Gamma(L_0, L_\varepsilon, L_H) \approx -\frac{1}{24}\left[\left(\frac{L_\varepsilon}{L_H}\right)^2 - \left(\frac{L_0}{L_H}\right)^2\right] \tag{10}$$

which is positive, leading to a positive MR. These results indicate that the negative MR occurs in high-stage GICs having interior G layers and a relatively small Boltzmann term. For $SbCl_5$ GICs and $MoCl_5$ GICs the relative magnitude of the Boltzmann term can be roughly estimated from the value of $\Delta\rho_c/\rho_0$ at $T = 4.2$ K and $H = 6.82$ kOe (see figure

7). The small positive values of $\Delta\rho_c/\rho_0$ near $n = 4$–6 for $SbCl_5$ GIC and near $n = 3$–6 for $MoCl_5$ GICs implies that the Boltzmann terms are small compared to those of the other stages. Because of the relatively large Boltzmann term a negative MR does not appear in stage-9 $SbCl_5$ GIC with many interior G layers. The negative MR in $MoCl_5$ GICs is very pronounced compared with that in $SbCl_5$ GICs, which is partly because of the relatively small Boltzmann term in $MoCl_5$ GICs. There may be another possibility: the condition $L_0 \ll L_H \ll L_\varepsilon$ is not sufficiently satisfied in $SbCl_5$ GICs, while it is satisfied in $MoCl_5$ GICs.

5. Conclusion

We have investigated the c-axis conduction mechanism of high-stage $SbCl_5$ GICs. The c-axis resistivity of $SbCl_5$ GICs consists of series connections of resistivities arising from regions of G–G and G–I–G along the c-axis. Because of the highly anisotropic resistivity, the carriers in the π-band stay mostly in the graphite basal plane and occasionally transfer to the neighbouring G layers. Thus the c-axis conduction of the regions G–G and G–I–G is determined mainly by the in-plane conduction of the related graphite layers. There are two kinds of graphite layer for high stage ($n \geqslant 3$): the bounding G layer with large charge transfer and the interior G layer with smaller charge transfer. Because of different amounts of charge transfer, the in-plane conductivity related to the interior G layers is much smaller than that related to the bounding G layers. The former can be detected from the c-axis resistivity, while the latter can be detected from the in-plane resistivity. The 2D weak localization effect occurs mainly in the interior G layers. The logarithmic behaviour at low temperatures and negative longitudinal MR appear in the c-axis resistivity, not in the in-plane resistivity.

Because of incomplete disproportionation there are $SbCl_3$, $SbCl_4^-$, $SbCl_5$, and $SbCl_6^-$ molecular species in the intercalate layers. The $SbCl_3$ molecular species undergoes a first-order phase transition between a $(\sqrt{39} \times \sqrt{39})R(16.1^\circ)$ commensurate structure at low temperatures and a liquid-like phase at high temperatures. The $SbCl_3$ molecule has a rather large electric dipole moment. When the carriers jump from one bounding G layer to the other bounding layer through the I layer they are scattered by a fluctuation due to the electric dipole moments located on the triangular lattice sites of the I layer. This fluctuation which is enhanced by the frustrated nature of this system depends on the degree of in-plane structural ordering for $SbCl_3$ molecules. The T-dependence of $\rho_c(T\uparrow)$ between 180 and 240 K suggests that the dipole moments of $SbCl_3$ molecules undergo two phase transitions at $T_{cl} = 196$–211 K and $T_{cu} = 223$–231 K. The low-temperature phase below T_{cl} is a 3D dipole ordered state. The intermediate phase between T_{cl} and T_{cu} is a 2D dipole ordered state.

There are still several problems unsolved for the c-axis conduction mechanism due to the fluctuations of electric dipole moment. It is a key to further understanding to study the ordering mechanism of electric dipole moments in $SbCl_5$ GICs.

Acknowledgments

The authors would like to thank A W Moore for providing them with HOPG samples. They are grateful to K Suzuki and K Gee for their help in sample preparation and c-axis resistivity measurements, and to C R Burr for critical reading of this manuscript. The work at SUNY at Binghamton was supported by NSF DMR 9201656.

References

[1] Morelli D T and Uher C 1983 *Phys. Rev.* B **27** 2477–9
[2] Piraux L, Issi J-P and Eklund P C 1985 *Solid State Commun.* **56** 413–5
[3] McRae E, Marêché J F, Bendriss-Rerhrhaye A, Lagrange P and Lelaurain M 1986 *Ann. Phys. Paris* **11** (Coll. Suppl. 2) 13–22
[4] Marêché J F, McRae E, Bendriss-Rerhrhaye A and Lagrange P 1986 *J. Phys. Chem. Solids* **47** 477–83
[5] McRae E, Marêché J F, Lelaurain M, Furdin G and Hérold A 1987 *J. Phys. Chem. Solids* **48** 957–63
[6] McRae E and Marêché J F 1988 *J. Mater. Res.* **3** 75–86
[7] McRae E, Lelaurain M, Marêché J F, Furdin G, Hérold A and Saint Jean M 1988 *J. Mater. Res.* **3** 97–104
[8] Andersson O E, Sundqvist B, McRae E, Marêché J F and Lelaurain M 1992 *J. Mater. Res.* **7** 2989–3000
[9] Sundqvist B, Andersson O E, McRae E, Lelaurain M and Marêché J F 1995 *J. Mater. Res.* **10** 436–45
[10] Sugihara K 1984 *Phys. Rev.* B **29** 5872–7
[11] Shimamura S 1985 *Synth. Met.* **12** 365–70
[12] Sugihara K 1988 *Phys. Rev.* B **37** 4752–9
[13] Sugihara K 1993 *J. Phys. Soc. Japan* **62** 624–33
[14] Suzuki M, Lee C, Suzuki I S, Matsubara K and Sugihara K 1996 *Phys. Rev.* B **54** 17 128–40
[15] Hwang D M 1990 *Graphite Intercalation Compounds I* ed H Zabel and S A Solin (Berlin: Springer) pp 247–81
[16] Hwang D M, Qian X W and Solin S A 1984 *Phys. Rev. Lett.* **53** 1473–6
[17] Homma H and Clarke R 1985 *Phys. Rev.* B **31** 5865–77
[18] Lelaurain M, Marêché J F, McRae E, Andersson O E and Sundqvist B 1992 *J. Mater. Res.* **7** 2978–88
[19] Boolchand P, Bresser W J, McDaniel D, Sisson K, Yeh V and Eklund P C 1981 *Solid State Commun.* **40** 1049–53
[20] Friedt J M, Poinsot R and Soderholm L 1984 *Solid State Commun.* **49** 223–7
[21] Yosida Y, Sato K, Suda K and Suematsu H 1986 *J. Phys. Soc. Japan* **55** 561–7
[22] Mélin J and Hérold A 1975 *Carbon* **13** 357–62
[23] Suzuki I S and Suzuki M 1991 *J. Phys.: Condens. Matter* **3** 8825–30
[24] Matsubara K, Sugihara K, Suzuki I S and Suzuki M 1997 unpublished
[25] Lee P A and Ramakrishnan T V 1985 *Rev. Mod. Phys.* **57** 287–337
[26] Lipka A 1979 *Acta Crystallogr.* B **35** 3020–2
[27] Kisliuk P 1954 *J. Chem. Phys.* **22** 86–92
[28] Suzuki M 1990 *Crit. Rev. Solid State Mater. Sci.* **16** 237–54
[29] Sugihara K, Matsubara K, Suzuki I S and Suzuki M 1997 unpublished
[30] Hikami S, Larkin A I and Nagaoka Y 1980 *Prog. Theor. Phys.* **63** 707–10
[31] Altshuler B L, Khemelnitskii D E, Larkin A I and Lee P A 1980 *Phys. Rev.* B **22** 5142–53
[32] Bergmann G 1984 *Phys. Rep.* **107** 1–58
[33] Kramer B, Bergmann G and Bruynseraede Y (eds) 1985 *Localization, Interaction, and Transport Phenomena (Springer Series in Solid-State Sciences 61)* (Berlin: Springer)